Van de Ven *et al. Geothermal Energy* (2025) 13:43
https://doi.org/10.1186/s40517-025-00367-0

Geothermal Energy

RESEARCH Open Access

Analytical modelling approach of ground freezing and thawing around ground heat collectors

Adinda Van de Ven[1*], Peter Bayer[2] and Roland Koenigsdorff[1]

*Correspondence:
vandeven@hochschule-bc.de

[1] Institute for Building and Energy Systems (IGE), Hochschule Biberach (HBC), Karlstraße 11, 88400 Biberach an der Riß, Germany
[2] Department of Applied Geology, Martin Luther University Halle-Wittenberg (MLU), Halle, Germany

Abstract

Ground heat collectors represent shallow geothermal devices that are buried in the upper metres of the ground with strong thermal coupling to ground surface. Therefore, during seasonal operation, heat extraction in winter can cause temporal freezing of the soil surrounding the collector. The transient latent heat transfer during freezing and thawing can be crucial for the performance of a collector, and it adds complexity to the model-based representation of the devices. Here, a novel analytical model is presented that accounts for these processes and simulates the evolution of thermal ground conditions during operation of different collector variants. It combines heat source-based solutions with thermal power balancing depending on a given collector geometry and temporal superposition for varying heat loads. By comparison with high-resolution numerical model results, the obtained fast analytical predictions represent the thermal regime around horizontal pipe installations and vertical planar trench collectors within seconds very well, achieving temperature deviations of less than 1.4 K and accuracies over 85.6% for predicting of the thickness of the frozen ground. This regime is inspected in particular with respect to collector wall temperature and the maximum horizontal extension of the frozen soil. The findings demonstrate the suitability of the new model framework to be used in the planning and design phase for optimal layout of collectors, as well for straightforward representation of complex freezing and thawing processes during operation.Please check and confirm that the authors and their respective affiliations have been correctly identified and amend if necessary.The affiliations are correctly. My lastname is corrected.Please check and confirm whether the city has been correctly identified in Affiliation 1.The City has been adapted as there is more than one City called Biberach in Germany.

Keywords: Trench collector, Horizontal ground heat collector, Phase change, Freezing, Thawing, Modelling

Introduction

The need for renewable heating solutions has contributed to a worldwide growth of the heat pump market, particularly of air-source heat pumps (Westring et al. 2024). However, in 2023, there was a notable decline in the overall sales of heat pumps across Europe (Westring et al. 2024). This can be attributed to various factors, such as energy price volatility, economic stagnation, political uncertainty, and regulatory challenges (Milagros Garcia Salciarini 2024). To enhance the attractiveness of especially ground-source

heat pumps, given their superior environmental performance compared to air-source systems, it is essential to maximise their operational reliability. One way to contribute to this is by competent design models, which is also the focus of this paper. More specifically, a new analytical modelling technique for ground heat collectors is introduced, taking into account freezing and thawing of the adjacent soil. This technique is based on the consistent modelling method defined in Van de Ven et al. (2018) for closed-loop shallow geothermal systems, which allows for the comparison of different source systems without deviations arising from varying modelling philosophies. This method draws on the established analytical model for borehole heat exchangers of Eskilson (1987) while generalising it for application to other closed-loop shallow geothermal systems. It divides the domain of interest into two parts:

1. The source system (including the installation situation).
2. The surrounding subsurface (including boundary effects at the ground surface).

The source system is modelled by analytical resistance models extended by capacity models if applicable. Whereas the surrounding subsurface is represented by extensions of the analytical solution of the instantaneous point source, e.g. continuous finite line source, cylinder source, ring source, etc. These source solutions can be extended by approximations if relevant thermal effects are not included in these fundamental solutions of potential theory. Furthermore, varying heat loads are considered by temporal superposition. (Van de Ven et al. 2018) This approach ensures that, when comparing different source systems (e.g. borehole heat exchanger, ground heat collector, etc.), the underlying modelling methodology remains consistent, and that differences in performance can be attributed to the system itself rather than to the modelling approach.

Ground heat collectors are closed-loop heat exchangers installed in a few metres depth to provide thermal energy for a heat pump heating system. Figure 1 illustrates the variety of different shapes of ground heat collectors. In contrast to the more widely used borehole heat exchangers (BHEs), ground heat collectors operate at lower temperatures during the heating period (winter) due to their exposure to seasonal temperature variations at the ground

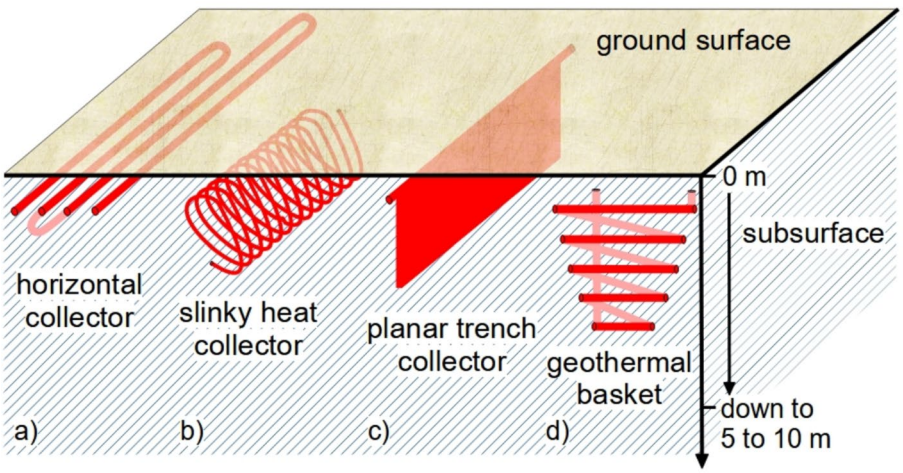

Fig. 1 Various types of ground heat collectors, including the two variants (a) and (c), which are the focus of this paper

surface. In addition, they interact with a smaller volume of soil compared to BHEs, resulting in lower heat storage capacity. These factors lead to operating temperatures falling below the freezing point for a substantial portion of the heating season. As a result, a significant part of the thermal energy extracted is gained from the latent heat which is released during freezing of water contained in the soil. Since significant interactions with the ground surface, such as heat transfer from the ambient air, solar radiation, and precipitation, govern the regeneration process, it is essential that such systems are installed beneath unsealed surfaces as long as no active thermal regeneration is applied (Koenigsdorff 2011). In addition to temperature restrictions, ground heat collectors must also meet the design criterion of ensuring that the frozen soil of adjacent collector pipes or plates do not merge (Verein Deutscher Ingenieure e.V. 2019). The reason for this is to ensure the infiltration of meltwater and rainwater to avoid the formation of mud accumulation. By complying with both criteria, excessive uplift and settlement caused by freezing and thawing of the soil is avoided.

The main advantage of analytical models is their computational efficiency, as they are faster and easier to apply than intricate numerical methods. Analytical models typically involve simplifications of the complex reality, such as an average effective thermal conductivity of the soil, or a uniform heat extraction rate over the entire ground source system (Stauffer et al. 2017; Lamarche 2023). These simplifications have proven suitable for planning the layout of BHEs, and they have been successfully employed for years in design tools, such as EWS, EED, and GLHEPro (Spitler et al. 2016; Blocon 2020; Huber 2016). In contrast, the operating conditions of ground heat collectors differ from those of the more widespread BHEs, as the latter extend much deeper into the ground, maintaining a relatively constant undisturbed subsurface temperature over the borehole length throughout the year. Furthermore, it is a distinctive feature of ground heat collectors that they induce freezing of the soil immediately surrounding the collector. This aspect is not considered in the analytical models for BHEs as it is irrelevant for their operation.

Within numerical models for geothermal energy systems, freezing and thawing of the soil is frequently neglected (Liu et al. 2025). It is more prevalent in models for construction and mining purposes, where artificial ground freezing is used to stabilise the subsurface and to avoid groundwater seepage (Zhou and Meschke 2013; Alzoubi et al. 2019; Huang et al. 2018). Two distinct methodologies are primarily employed in these models to represent the freezing and thawing in the soil: the apparent heat capacity method and the enthalpy method (Liu et al. 2025). The apparent heat capacity method incorporates the latent heat of the phase change into the material's heat capacity over a defined temperature range (Yang et al. 2015). This method is implemented in COMSOL Multiphysics' phase change material (COMSOL Multiphysics® 2019). This approach is more frequently employed as it simpler and easier to implement, although the exact phase boundary cannot be tracked (Liu et al. 2025). The enthalpy method is more complex as it accounts for the latent heat phase change into the energy conservation equation. With this method, a mushy region is introduced between the two phases to avoid sharp discontinuities (Jiménez-Xamán et al. 2019). In the context of closed-loop shallow geothermal systems, only a limited number of numerical models incorporate subsurface phase change processes alongside the operation of the heat source system. Liu et al. (2025) analyses the performance of coaxial borehole heat exchangers under soil freezing conditions by applying the apparent heat capacity method in a finite difference

framework. The apparent heat capacity method is also employed by Yang et al. (2015) in their 2D model to evaluate the influence of soil freezing on ground heat exchangers. Eslami-Nejad and Bernier (2012) likewise used the apparent heat capacity method for their one-dimensional radial numerical heat transfer model. This 1D model is coupled with a borehole heat exchanger model to investigate the effect of ground freezing on the borehole wall temperature. Arzanfudi and Al-Khoury (2018) on the other hand use the enthalpy method in their model to evaluate the processes occurring in the vicinity of energy piles. Bottarelli et al. (2015) presented a ground heat collector model, which includes freezing in the subsurface considering the phase change of water and an addition phase change material. As in this study, an additional phase change material is added by mixing water and micro-encapsulated paraffin with the soil, which is then used as backfill material for the trench. Accordingly, heat extraction from the subsurface in this case is facilitated by two materials undergoing phase transition. Therefore, the numerical model was simplified to a heat conduction model with an equivalent solid domain, which combines all relevant thermal properties (Bottarelli et al. 2015). Gan (2013) developed a numerical model for a horizontal ground heat exchanger, where freezing and thawing are included within the energy conservation equation. According to their investigations, the specific heat extraction rate increases up to 8.6% (Gan 2013). Hüsing et al. (2016) developed a finite difference model for a horizontal ground heat exchanger in TRNSYS, which accounts for ground freezing. They apply the apparent heat capacity method to model phase change in the subsurface in their 2D simulation (Hüsing et al. 2018). Moreover, they claim that their model represents an improvement over existing numerical models for horizontal ground heat exchangers proposed by Giardina (1995), Ramming (2007) and Glück (2009). Hirsch et al. (2019) developed a numerical model for ground heat exchangers in DELPHIN, highlighting that moisture transport and ice formation are taken into account. However, they share little information on how freezing is represented in the model.

Existing analytical models for ground heat collectors commonly consider heat conduction in the subsurface—for example, Claesson and Dunand (1983) for horizontal pipes, Li et al. (2012a) for slinky-coil ground heat exchanger and Jeon et al. (2018) for spiral-coil ground heat exchanger or geothermal baskets. Some analytical models consider additional effects such as seasonal temperature variation and the air–soil boundary effect (Ciriello et al. 2015; Lamarche 2019; Wang et al. 2016; Bahmani and Hakkaki-Fard 2022) or freezing and thawing due to heat transfer to and from the surface (Xiong et al. 2015). Although Xiong et al. (2015) account for freezing and thawing at the surface for the calculation of the undisturbed ground temperature, their approach does not capture the soil freezing and thawing occurring around the collector pipes. In addition, the model representing the undisturbed ground temperature is a numerical one, which is subsequently superposed with the analytical ring source model. Previous studies have applied thermal response tests to ground heat collectors for model-based estimation of soil parameters (Van de Ven et al. 2022, 2023; Urresta et al. 2021). Beyond that, the impact of groundwater advection on the operation of a slinky-coil heat exchanger has been investigated (Li et al. 2012b).

Freezing and thawing are crucial heat transfer processes for all kinds of ground heat collectors that use the latent heat of the soil moisture. The governing differential equations

for these processes are nonlinear and not included in the fundamental solution of potential theory (Carslaw and Jaeger 1959), which is widely used in the form of the continuous infinite or finite (moving) line source [ILS or F(M)LS] [ILS: (Spitler and Gehlin 2015); IMLS: (Sutton et al. 2003; Wagner et al. 2013); FLS: (Abdelaziz et al. 2014; Lamarche 2019; Fontaine et al. 2011); FMLS: (Erol and François 2018; Molina-Giraldo et al. 2011)], the infinite or finite plane source (IPS or FPS) [IPS: (Gupta et al. 2022); FPS: (Van de Ven et al. 2024)], or the ring source (Li et al. 2012a; Xiong et al. 2015; Witte et al. 2022) for dimensioning of shallow geothermal systems. To our knowledge, one analytical model exists, which simulates both the operational temperature and the propagation of the frozen ground (Ramming 2007). However, the model of Ramming (Ramming 2007) focuses only on different pipe configurations and does not conform to the consistent modelling approach as defined in Van de Ven et al. (2018). The consistent modelling approach only allows completely coupled fundamental solutions of potential theory (Carslaw and Jaeger 1959) supplemented by approximations not included in potential theory. Ramming (2007) primary focusses on horizontal ground heat collector consisting of pipes installed horizontally in the soil, for which a detailed analytical model has been developed. While additional collector configurations are discussed, their actual geometries are only approximated and treated as variations of the horizontal pipe model. These approaches involve assumptions that are not further verified. Furthermore, the analytical model proposed by Ramming (2007) cannot be suitably adapted to align with the consistent modelling framework described above and is, therefore, excluded as a basis for comparative analysis of different source systems.

The presented study closes this gap and introduces an approximate solution for analytical simulation of the subsurface freezing caused by geothermal heat collector operation. In the following, a general formulation is presented that is subsequently specified for two geometric collector variants. A detailed numerical implementation is employed for comparison and exemplary calculations are presented to reveal the suitability of the analytical approach.

Materials and methods

Analytical model

General approach

The analytical model is set up to simulate different collector configurations that operate in shallow ground in the vicinity of the ground surface. The initial temperature of the ground in the height range of the collector is assumed to be above freezing temperature and no previous geothermal use is considered. For above-freezing temperatures solely source solutions are used to calculate the temperature field around the ground heat collector. The use of source solutions provides consistency with established model methods in shallow geothermal applications, e.g., BHEs (Eskilson 1987; Cimmino et al. 2013). Given the solution for a basic step pulse with a constant heat load, the temperature difference from the initial value $T = 0$ is calculated and a varying heat extraction rate is accounted for by superposition. The corresponding absolute temperature resulting from one step pulse with its starting time set to $t{=}0$ is

$$T(t,x,y,z) = d\dot{q}\theta(t,x,y,z). \tag{1}$$

Specifically, T is the solution for a given source geometry (point, line, plane, ring, etc.) at the time t and the location x, y, z. The applied constant heat extraction or

injection rate $\dot{q}$ is defined in W/m or W/m^2 depending on the selected collector geometry. In Eq. (1), d is the dimensional factor belonging to the dimensionless temperature response θ. Both, d and θ depend on the main geometry of the model, i.e., line, plane, ring, etc. The dimensionless temperature response depends on further dimensionless parameters. The unit of the dimensional factor is related to the unit of $\dot{q}$ and can be in m K/W or m^2 K/W. Subsequently, the dimensional factor is specified with a subscript, d_{unfr} and d_{fr}, in which it considers the properties of the unfrozen and frozen ground, respectively. The equations defining the dimensional factors are specified in detail in "Horizontal pipe" and "Planar trench collector" sections.

The resulting temperature field calculated with Eq. (1) is superposed with seasonal temperature variations and a collector resistance model. The natural seasonal varying ground temperature depending on its depth $T_{\text{g},0}(t,z)$ is calculated by Kusuda and Achenbach (1965):

$$T_{\text{g},0}(t,z) = \overline{T}_{\text{a}} - \Delta T_{\text{am}} \exp\left(-z\sqrt{\frac{\pi}{t_{\text{p}}a}}\right) \cos\left(\frac{2\pi}{t_{\text{p}}}\left[t - t_0 - \frac{z}{2}\sqrt{\frac{t_{\text{p}}}{\pi a}}\right]\right) \tag{2}$$

The phase constant t_0 in Eq. (2) corresponds to the time of the year in seconds at which the temperature of the ground surface reaches its minimum. The considered time period t_{p} is 1 year, as after this period the seasonal oscillation restarts. This oscillation with the amplitude ΔT_{am} is subtracted from the annual mean air temperature $\overline{T}_{\text{a}}$. Furthermore, z is the considered depth in metres, t corresponds to the considered time of the year, and a represents the thermal diffusivity of the subsurface in m^2/s. If the collector extends over a few tenths of a metre in depth, it is reasonable to average the undisturbed ground temperature over the collector height, as presented in Van de Ven et al. (2024).

This modelling approach uses the temporal superposition technique to apply a realistic heat load profile. This technique makes it possible to take the effects of previous heat loads into account, and thus, it can be used to model the history of previous thermal loads (Eskilson 1987). Here, the solution is again defined as the temperature difference with respect to an initial temperature of 0. Thus, this can also be written as an absolute temperature $T(t)$ in Eq. (3). Since the model is applied in discrete, equidistant time steps, the temporal superposition is formulated stepwise in time, with n being the number of the considered time steps and Δt the time step interval:

$$T(n\Delta t) = \sum_{i=1}^{n} d\dot{q}_{\theta}(i\Delta t)[\theta((n-i+1)\Delta t) - \theta((n-i)\Delta t)] \tag{3}$$

$$T(n\Delta t) = d\dot{q}_{\theta}(n\Delta t)\theta(\Delta t) + T_{\text{hist}}(n\Delta t) \tag{4}$$

with

$$T_{\text{hist}}(n\Delta t) = \sum_{i=1}^{n-1} d_{\text{unfr}}\dot{q}_{\theta}(i\Delta t)[\theta((n-i+1)\Delta t) - \theta((n-i)\Delta t)] \tag{5}$$

and

$$\theta(0) = 0 \tag{6}$$

Here, $\dot{q}_\theta$ is the conductive heat injection or extraction rate in W/m or W/m^2. $T_{\text{hist}}(n\Delta t)$ represents the impact of previous thermal loads from the time step 1 to $n-1$ at the specified time ($n\Delta t$). Equation (3) is rewritten in Eq. (4) as a decomposition of a contribution from the past $T_{\text{hist}}(n\Delta t)$ and the current time step ($d_{\text{unfr}}\dot{q}_\theta(n\Delta t)\theta(\Delta t)$). This decomposition into a past and current component in Eq. (4) is intended for the modelling of ground freezing. In the case of freezing, the history-dependent term is evaluated using the dimensional factor corresponding to the unfrozen state d_{unfr}, whereas the current time step reflects the prevailing phase of the soil and is calculated differently, as described later by Eq. (13). Evaluating the history term based on the unfrozen dimension parameter represents a methodological simplification designed to reduce computational complexity. This, however, may lead to discrepancies compared to actual physical behaviour. Equations (3), (4) and (5) apply for equidistant time steps with constant heat injection or extraction rates within each time step. Furthermore, the corresponding dimensionless temperature response must be used, i.e., the dimensionless variables must match both the collector geometry and the desired evaluation point. By superposing Eqs. (2) and (3), the collector wall temperature T_{cw} can be determined at each point in time under consideration by Eq. (7) as long as the resulting temperature, T_{cw}, is above freezing temperature T_{lat}:

$$T_{\text{cw}}(n\Delta t) = T_{\text{g,0}}(n\Delta t, z) + d\dot{q}_\theta(n\Delta t)\theta(\Delta t) + T_{\text{hist}}(n\Delta t) \tag{7}$$

$T_{\text{g,0}}(n\Delta t, z)$ can be replaced by the average of the undisturbed ground temperature over the collector height, if necessary. In addition to Eq. (7), a heat balance at the collector wall is applied, where the total heat flow rate $\dot{q}_{\text{tot}}$ extracted, or injected, by the collector is divided into the conductive heat flow rate between the ground and the collector wall $\dot{q}_\theta$ and the latent heat flow rate $\dot{q}_{\text{lat}}$.

$$0 = \dot{q}_{\text{tot}}(n\Delta t) + \dot{q}_{\text{lat}}(n\Delta t) - \dot{q}_\theta(n\Delta t) \tag{8}$$

The total heat flow rate, $\dot{q}_{\text{tot}}$, is negative when heat is extracted and becomes positive when heat is injected. The same applies for the conductive heat flow rate $\dot{q}_\theta$. The latent heat flow rate $\dot{q}_{\text{lat}}$, in contrast, is positive during the formation of ice and turns negative as the frozen ground thaws. As soon as the subsurface freezes, i.e., $T_{\text{cw}} < T_{\text{lat}}$, the conductive heat flow rate, $\dot{q}_\theta$, is divided into an unfrozen and a frozen conductive heat flow rate, $\dot{q}_{\theta,\text{unfr}}$ and $\dot{q}_{\theta,\text{fr}}$, respectively. Both sum up to the conductive heat flow rate $\dot{q}_\theta$:

$$\dot{q}_\theta(n\Delta t) = \dot{q}_{\theta,\text{unfr}}(n\Delta t) + \dot{q}_{\theta,\text{fr}}(n\Delta t) \tag{9}$$

The modelling approach distinguishes four cases:

I. No frost is present at the beginning of the current time step, and no freezing occurs within in the current time step n.
II. No frost is present at the beginning of the current time step, but the soil adjacent to the collector wall starts freezing within the current time step.
III. Frost is present at the beginning of the current time step, and the subsurface freezes further or partially thaws with residual frost within the current time step.

IV. Frost is present at the beginning of the current time step, and the subsurface thaws completely within the current time step.

In case I, i.e., for temperatures above the freezing point, the latent heat flow rate $\dot{q}_{\text{lat}}$ is zero, and thus, the conductive heat flow rate, $\dot{q}_{\theta}$, equals the total heat flow rate $\dot{q}_{\text{tot}}$. The collector wall temperature can directly be calculated with Eq. (7) and $d = d_{\text{unfr}}$. Once the collector wall temperature drops below the freezing temperature, the latent heat flow rate, $\dot{q}_{\text{lat}}(t)$, is used as a source term, which stores heat during freezing and releases the stored heat during thawing.

In case II, when the collector wall temperature falls below the freezing temperature, the frozen conductive heat flow rate for the current time step $\dot{q}_{\theta,\text{fr}}(n\Delta t)$ is set to zero. The unfrozen part of the conductive heat flow rate is determined by setting the collector wall temperature equal to the freezing temperature and using the unfrozen properties for the dimensional factor, i.e., $d = d_{\text{unfr}}$, in Eq. (7). Thus, the resulting equation for the conductive heat flow rate in the unfrozen subsurface $\dot{q}_{\theta,\text{unfr}}$ is

$$\dot{q}_{\theta,\text{unfr}}(n\Delta t) = \frac{T_{\text{lat}} - (T_{\text{g},0}(n\Delta t, z) + T_{\text{hist}}(n\Delta t))}{d_{\text{unfr}}\theta(\Delta t)} \tag{10}$$

Since $\dot{q}_{\theta,\text{fr}}$ in case II is zero, $\dot{q}_{\theta}$ equals $\dot{q}_{\theta,\text{unfr}}$. Given the known value of the conductive heat flow rate, $\dot{q}_{\theta}$, Eq. (8) can be solved for the latent heat flow rate, $\dot{q}_{\text{lat}}$, leading to:

$$\dot{q}_{\text{lat}}(n\Delta t) = q_{\theta}(n\Delta t) - \dot{q}_{\text{tot}}(n\Delta t) \tag{11}$$

Subsequently, the scale-representative amount of frozen soil built up in the current time step, $\Delta\text{Fr}(t)$, can be calculated as follows:

$$\Delta\text{Fr}(n\Delta t) = \frac{\dot{q}_{\text{lat}}(n\Delta t)\Delta t}{h_{\text{lat}}\phi\rho_{\text{ice}}}. \tag{12}$$

Here, h_{lat} is the phase change enthalpy of the groundwater, ϕ is the porosity of the subsurface, and ρ_{ice} is the density of the frozen soil water. Since the representative amount of frozen soil built up in the current time step, $\Delta\text{Fr}(n\Delta t)$, i.e., the change in amount of frozen soil, directly depends on the heat extraction or injection rates $\dot{q}_{\text{tot}}$, and thus, on the associated geometry model, it is expressed either in m or m^2. A frozen quantity expressed in metres, for instance, refers to the distance perpendicular to the collector wall. A more detailed explanation follows in subsequent "Horizontal pipe" and "Planar trench collector" sections. For case II, the change in frozen soil, $\Delta\text{Fr}(n\Delta t)$, equals the overall amount of frozen soil at the considered time, $\text{Fr}(n\Delta t)$. Once the total amount of frozen soil until the current time is determined, the maximum extent of the frozen area can be calculated. This is highly dependent on the geometry of the collector, i.e., the specific geometry model, and, therefore, cannot be generalised. It must be individually determined for each collector configuration. The collector wall temperature, T_{cw}, for temperatures below the freezing point, T_{lat}, is calculated by simple, two-dimensional (2D) heat conduction equations using corresponding shape factors, $S(n\Delta t)$, as follows:

$$T_{\text{cw}}(n\Delta t) = T_{\text{lat}} + d_{\text{fr}}\dot{q}_{\theta}(n\Delta t)S(n\Delta t) \tag{13}$$

Similar to the dimensional factor d_{fr}, the shape factor $S(n\Delta t)$ depends on the geometry model as well but is dimensionless. The temporal dependence of the shape factor is determined by the extent of frozen ground, which changes with time. The temperature gradient between the frost isotherm and the collector wall is calculated using the heat conduction equation, with the frost isotherm assumed to be at the boundary of the frozen soil.

Case III covers both the further freezing and partial thawing of the subsurface. This means, that a specific amount of frozen soil, Fr, is already present and the collector wall temperature, T_{cw}, is below the freezing point, T_{lat}. The only distinction from the previous case is that the frozen conductive heat flow rate $\dot{q}_{\theta,\mathrm{fr}}$ is non-zero and calculated as follows:

$$\dot{q}_{\theta,\mathrm{fr}}(n\Delta t) = \frac{T_{\mathrm{cw}}((n-1)\Delta t) - T_{\mathrm{lat}}}{d_{\mathrm{fr}}\theta(\Delta t)} \tag{14}$$

The unfrozen conductive heat flow rate, $\dot{q}_{\theta,\mathrm{unfr}}$, is to be calculated with Eq. (10). By applying the result into Eqs. (9), (11), and (12), the latent heat flow rate, $\dot{q}_{\mathrm{lat}}$, and the amount of frozen soil built up in the current time step, $\Delta\mathrm{Fr}$, can be determined. If the sum of the change in the amount of frozen soil, $\Delta\mathrm{Fr}(n\Delta t)$, and the frozen soil from the previous time step, $\Delta\mathrm{Fr}((n-1)\Delta t)$, is greater than or equal to zero, the total amount of frozen soil at the current time step, $\mathrm{Fr}(n\Delta t)$, can be determined as follows:

$$\mathrm{Fr}(n\Delta t) = \mathrm{Fr}((n-1)\Delta t) + \Delta\mathrm{Fr}(n\Delta t) \tag{15}$$

Similar to case II, the collector wall temperature for case III can be computed using Eq. (13).

Upon thawing of the soil, i.e., for case IV, the change of the amount of frozen soil at the current time step will lead to a value below zero for the total amount of frozen soil. Thus, similar to case III, the heat balance model is based on Eq. (8) and solved for the latent heat flow rate, $\dot{q}_{\mathrm{lat}}$. This is done by applying Eqs. (10) and (14), allowing the determination of the change in amount of frozen soil, $\Delta\mathrm{Fr}$. If case IV applies, the entire soil thaws, leading to the following change in the amount of frozen soil:

$$\Delta\mathrm{Fr}(n\Delta t) = \mathrm{Fr}((n-1)\Delta t)(-1) \tag{16}$$

By applying Eq. (15), the amount of frozen soil in the current time step of 0 is obtained. In the time step during which the soil undergoes complete thawing, the latent heat injection rate can be determined with the defined change of the frozen soil amount by reformulating Eq. (12) as follows:

$$\dot{q}_{\mathrm{lat}}(n\Delta t) = \Delta\mathrm{Fr}(n\Delta t)h_{\mathrm{lat}}\phi\rho_{\mathrm{ice}}\Delta t \tag{17}$$

Furthermore, Eq. (14) can still be applied to determine the frozen conductive heat injection rate at the time step in which the complete soil thaws, whereas the unfrozen conductive heat injection rate must be determined by balancing the heat rates from Eq. (8) and solving for the unfrozen conductive heat injection or extraction rate, $\dot{q}_{\theta,\mathrm{unfr}}$:

$$\dot{q}_{\theta,\mathrm{unfr}}(n\Delta t) = q_{\mathrm{lat}}(n\Delta t) + \dot{q}_{\mathrm{tot}}(n\Delta t) - q_{\theta,\mathrm{fr}}(n\Delta t) \tag{18}$$

The collector wall temperature, however, can be determined using Eq. (7) in the time step during which the soil undergoes complete thawing.

The calculation algorithm, incorporating all defined four cases, is presented in the flow chart in Fig. 2.

The described methodology is exemplified for a horizontal pipe and a planar trench collector in the following sections.

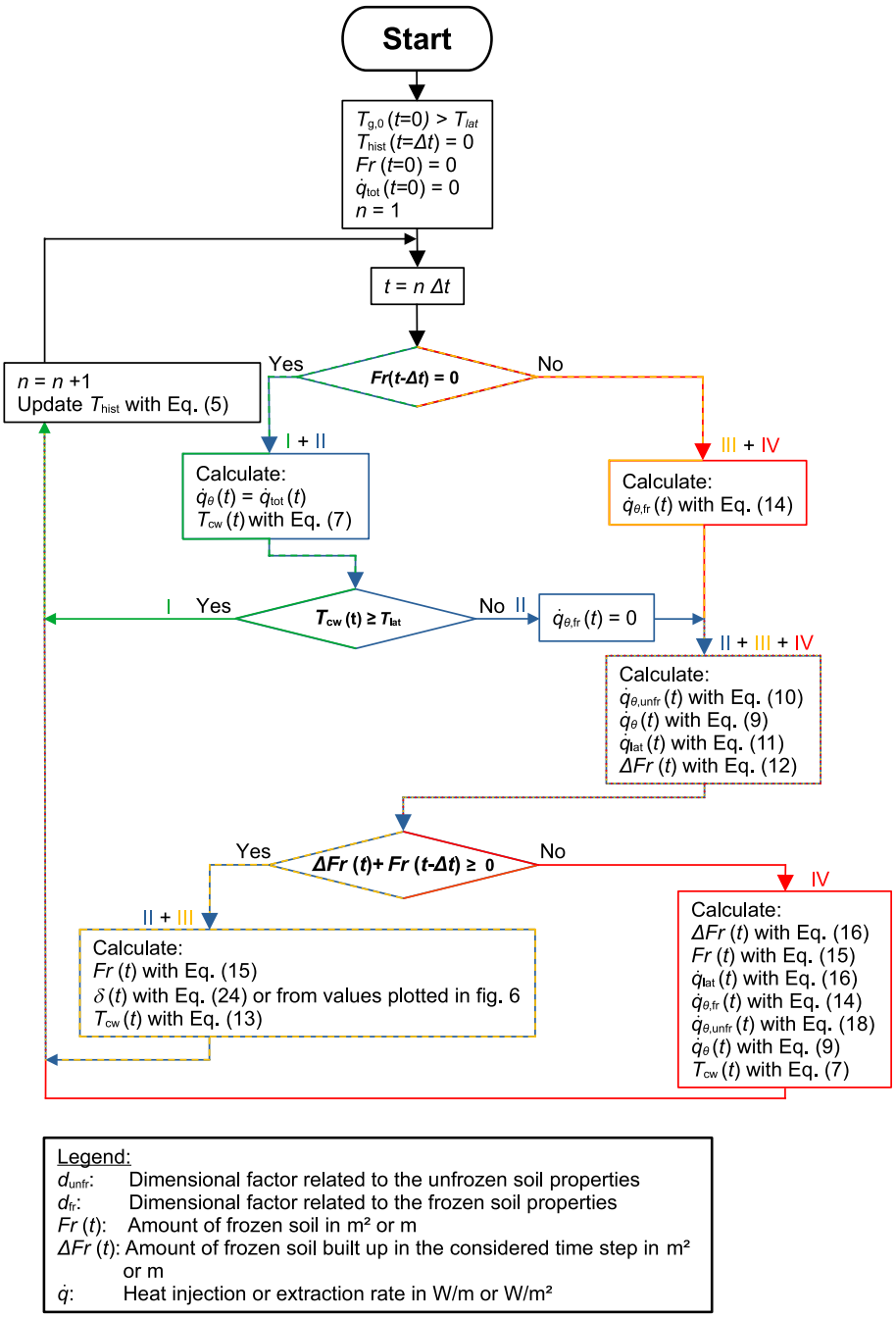

Fig. 2 Flow chart of the calculation algorithm

Horizontal pipe

The source solution used for the analytical simulation of a horizontal pipe is the 2D, ILS model with an isothermal boundary condition at the ground surface. The ILS is located parallel to the ground surface as depicted in Fig. 3. For the applied 2D model, the units of $\dot{q}$, d, ΔFr, and Fr, are W/m,m K/W, m^2, and m^2, respectively.

The mathematical solution of the ILS with an isothermal boundary condition can be deduced from the point source. Similar as in Eq. (1), it is formulated as an absolute temperature (Carslaw and Jaeger 1959):

$$T(x,z,t) = -\frac{\dot{q}}{4\pi\lambda}\left[\mathrm{Ei}\left(-\frac{(x-x')^2+(z-z')^2}{4at}\right) - Ei\left(-\frac{(x-x')^2+(z+z')^2}{4at}\right)\right] \tag{19}$$

Here, x and z represent the coordinates of the evaluation point at which the temperature is calculated as depicted in Fig. 3, t is the time in seconds that has elapsed, since the heat load was applied, $\dot{q}$ is the heat extraction (negative) or injection (positive) rate in W/m, λ is the thermal conductivity of the subsurface, Ei is the exponential integral, x' and z' indicate the location of the source and a is the thermal diffusivity of the subsurface in m^2/s. This source model is used for the heat conduction in the subsurface as described in "General approach" section. The dimensionless form of Eq. (19), which is needed as an input for the general approach, is

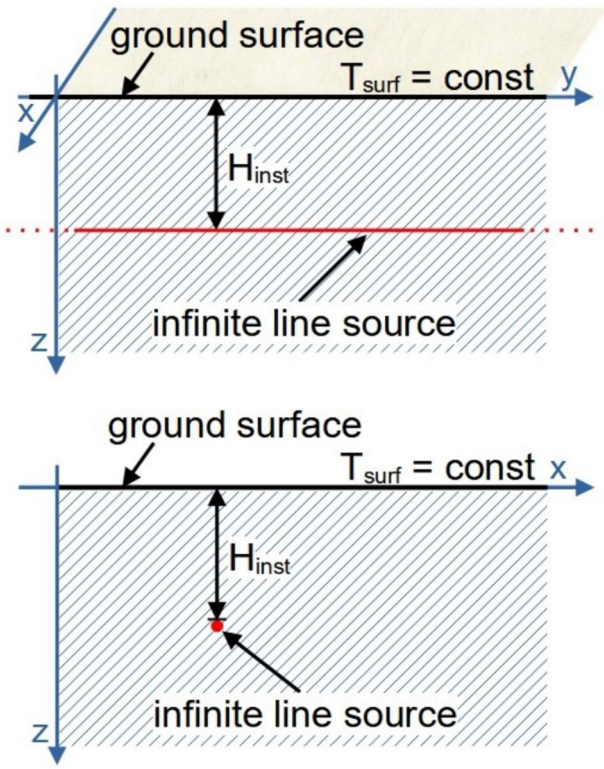

Fig. 3 Infinite line source with an isothermal boundary condition at the ground surface

$$\theta(t) = -\frac{1}{2}\left[Ei\left(-\frac{(x-x')^2+(z-z')^2}{4at}\right) - Ei\left(-\frac{(x-x')^2+(z+z')^2}{4at}\right)\right] \tag{20}$$

Furthermore, d_{unfr} and d_{fr} are defined in Eqs. (21) and (22) for the ILS model:

$$d_{\text{unfr}} = \frac{1}{2\pi\,\lambda_{\text{unfr}}} \tag{21}$$

$$d_{\text{fr}} = \frac{1}{2\pi\,\lambda_{\text{fr}}} \tag{22}$$

Here, both dimensional factors have the unit m K/W. With Eqs. (20) and (21) or (22), Eq. (19) can be reformulated as follows:

$$T(n\Delta t) = \dot{q}_{\theta,\text{unfr/fr}} d_{\text{unfr/fr}} \theta(n\Delta\, t) \tag{23}$$

Within the calculation algorithm, Eq. (23) represents a reformulation of Eqs. (10) and (14) corresponding to the formula structure of Eq. (19). Thus, it is primarily used to divide the heat extraction or injection rate into frozen and unfrozen fractions.

Ground heat collectors are generally installed at frost-free depths; in addition, their minimum collector outlet temperature should not fall below −5 °C (Verein Deutscher Ingenieure e.V. 2019). This combination results in a nearly radial symmetry of the formation of the frozen ground, as can be seen in Fig. 4. However, if the collector is positioned very close to the surface, limiting the amount of heat flowing in from above during the heating season, this symmetry is disrupted. In such cases, the expansion of the frozen ground takes on a droplet-like shape, as can be seen in Fig. 5 for a horizontal pipe installed in 20 cm depth. This installation depth leads to a non-homogeneous temperature distribution around the collector pipe.

In this model a radially symmetric freezing of the subsurface around the collector pipe is assumed. With r_{pipe} being the pipe radius in m, A_{pipe} being the cross-sectional area of the pipe, and the total amount of frozen ground being $\text{Fr}(t)$, the frozen distance $\delta(n\Delta t)$ in m between the pipe wall and the frost isotherm, T_{lat}, is determined:

$$\delta(n\Delta t) = \sqrt{\frac{\text{Fr}(n\Delta t) + A_{\text{pipe}}}{\pi}} - r_{\text{pipe}} \tag{24}$$

The shape factor for the horizontal pipe with freezing of the subsurface is determined based on the well-known formula for heat conduction in concentric circles (VDI-Gesellschaft Verfahrenstechnik und Chemieingenieurwesen 2013):

$$\Delta T = \frac{\dot{q}}{2\pi\,\lambda}\ln\left(\frac{r_{\text{outer}}}{r_{\text{inner}}}\right) \tag{25}$$

By combining Eqs. (13) and (25), the shape factor for the horizontal pipe is determined as follows:

$$S(t) = \ln\left(\frac{\delta(n\Delta t) + r_{\text{pipe}}}{r_{\text{pipe}}}\right) = \ln\left(\frac{\delta(n\Delta t)}{r_{\text{pipe}}} + 1\right) \tag{26}$$

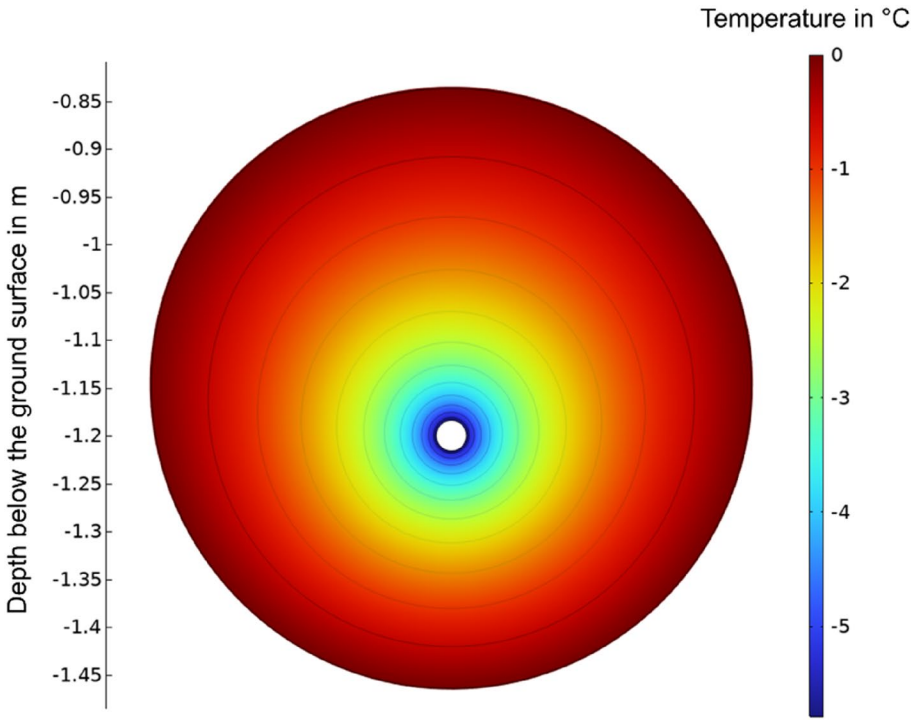

Fig. 4 Temperature distribution around a horizontal pipe including the seasonal temperature variation at the surface and after a heat extraction of 2000 h

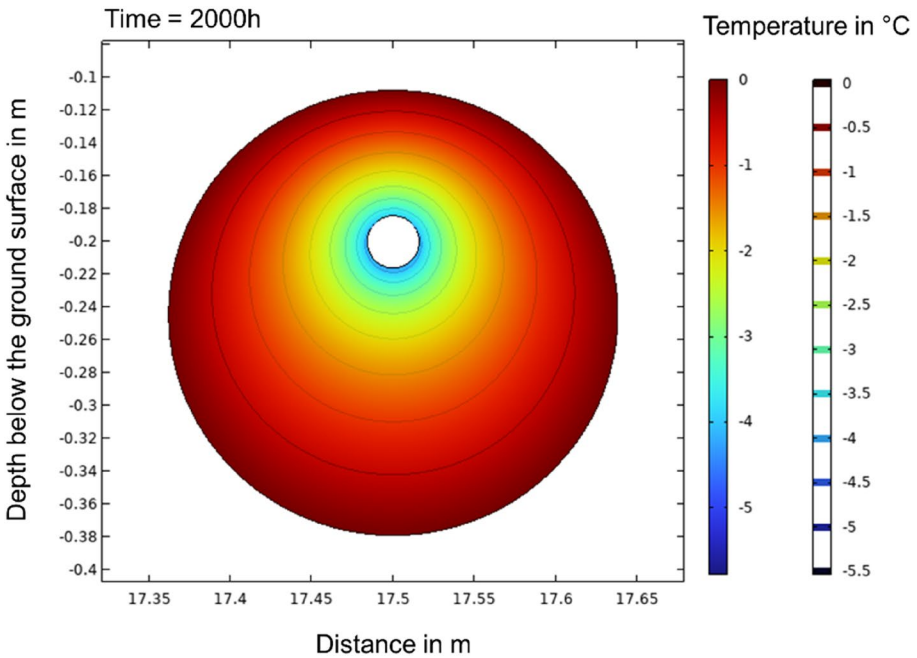

Fig. 5 Temperature distribution around a horizontal pipe installed at 20 cm depth with seasonal temperature variation at the surface and after a heat extraction of 2000 h

This approach is valid as long as freezing of the ground develops closely to the radial symmetry assumed here. If the shape of the frozen ground deviates significantly from radial symmetry, the model becomes increasingly imprecise.

Using this straightforward model, a horizontal pipe that serves as a geothermal ground collector can be efficiently and accurately designed while accounting for the freezing of the subsurface. However, it is crucial to select appropriate time step sizes to ensure that the steady-state condition of the shape factor is achieved. Failure to do so will lead to instability in the method, as the growth of the frozen radius is initially overestimated, which is subsequently corrected by thawing the frozen radius in the following step. This correction, in turn, leads to an overestimation of the thawing process, thereby exacerbating the error and initiating a cycle of continuously overestimating the freezing or thawing process. Therefore, the lower limit for the time step duration of the analytical solution for the horizontal pipe is 4 h. This time step size is applied in the exemplary application studies presented below, as it provides stable results for the chosen parameters without compromising accuracy.

Planar trench collector

The analytical model employed for heat conduction in the subsurface for planar trench collectors is the analytical FPS model, which is described in Van de Ven et al. (2024). The units of $\dot{q}$ and d are $\mathrm{W/m^2}$ and $\mathrm{m^2\,K/W}$, respectively. The dimensionless temperature response of the FPS model is expressed as follows:

$$\theta(t) = \frac{1}{4\pi L_c H_c H_{tot}} \int_0^{L_c} \int_{H_{inst}}^{H_{inst}+H_c} \int_0^{L_c} \int_{H_{inst}}^{H_{inst}+H_c} \left(\frac{\operatorname{erfc}\left(\frac{\sqrt{(x-x')^2+(y-y')^2+(z-z')^2}}{2\sqrt{at}}\right)}{\sqrt{(x-x')^2+(y-y')^2+(z-z')^2}} - \frac{\operatorname{erfc}\left(\frac{\sqrt{(x-x')^2+(y-y')^2+(z+z')^2}}{2\sqrt{at}}\right)}{\sqrt{(x-x')^2+(y-y')^2+(z+z')^2}} \right) \mathrm{d}z'\mathrm{d}x'\mathrm{d}z\mathrm{d}x \tag{27}$$

Here L_c, H_c, H_{inst}, and H_{tot} represent the collector dimensions, i.e., its length, its height, its installation depth, and its overall depth, respectively. erfc is the complementary error function, (x, y, z) describe the evaluation plane, and (x', y', z') define the location of the plane source. More detailed information on the FPS model can be found in Van de Ven et al. (2024). Furthermore, the dimensional factors for this model are defined as

$$d_{unfr} = \frac{H_{tot}}{\lambda_{unfr}} \tag{28}$$

$$d_{fr} = \frac{H_{tot}}{\lambda_{fr}} \tag{29}$$

To determine the maximum horizontal extension of the frozen ground for planar trench collectors, a so-called equivalent volume $V_{fr,eq}$ is calculated based on amount of the frozen ground, Fr. It is assumed that the expansion of the frozen volume occurs in all three dimensions, i.e., the distance perpendicular to the collector wall of the frozen layer corresponds to Fr and both the collector length L_c and the collector height H_c are

lengthened by Fr as well. Consequently, the equivalent frozen volume for the determination of the maximum extension of the frozen ground is described by

$$V_{\mathrm{fr,eq}}(n\Delta t) = \mathrm{Fr}(n\Delta t)(L_{\mathrm{c}} + \mathrm{Fr}(n\Delta t)(H_{\mathrm{c}} + \mathrm{Fr}(n\Delta t)) \tag{30}$$

The maximum horizontal extension of the frozen ground, δ, is defined based on various steady-state, three-dimensional (3D), numerical simulations for the considered collector geometry and various thermal conductivities of the solid matrix. To minimise errors from correlation curves, the maximum extension of the frozen ground is directly determined through linear interpolation of the simulated results for a given equivalent frozen volume $V_{\mathrm{fr,eq}}$. The results of the numerical, steady-state simulations used for the linear interpolation are shown in Fig. 6. The figure illustrates that the maximum horizontal extension of the frozen ground is independent of the soil properties.

However, for the calculation of the collector wall temperature, a dimensional transition occurs. As in the horizontal pipe model, the shape factor that is applied for the heat conduction between the collector wall temperature T_{cw} and the freezing isotherm T_{lat} is derived in analogy to the well-known 2D steady-state solution of heat conduction in a plane wall. Applied to the distance L_{fr} between the collector wall temperature T_{cw} and the freezing isotherm T_{lat}, this yields the following equation (Incropera et al. 2013):

$$T_{\mathrm{cw}} - T_{\mathrm{lat}} = \frac{\dot{q}}{\lambda} L_{\mathrm{fr}} \tag{31}$$

By transforming Eq. (31) into Eq. (13), the shape factor S can be determined directly. However, it should be pointed out that L_{fr} represents the distance between the mean temperature at the collector wall and the freezing isotherm, i.e., it represents half of the

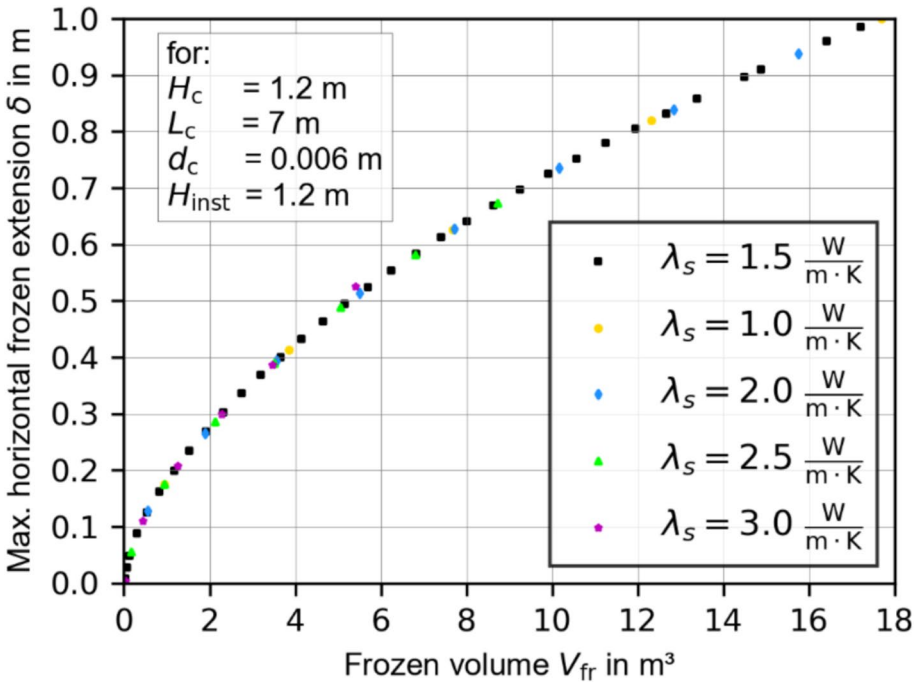

Fig. 6 Relationship between frozen volume and maximum horizontal extension of the frozen ground, based on steady-state 3D numerical simulations for various thermal conductivities

scale-representative amount of the frozen ground, Fr(t)/2, as on both sides of the collector the ground freezes. Furthermore, it is important to note that, in the context of heat conduction, not only the scale-representative amount of frozen ground Fr(t) must be halved, but also the heat extraction or injection rate $\dot{q}$, as the thermal power acts on both sides of the collector. Consequently, the shape factor can be defined as follows:

$$S(n\Delta t) = \frac{\mathrm{Fr}(n\Delta t)}{4H_{\mathrm{tot}}} \tag{32}$$

As previously noted for the horizontal pipe model, selecting the appropriate time step is crucial for the analytical trench collector model as well. Therefore, the lower limit of the time step size for this collector is a 48-h size. This time step duration is employed to ensure reliable results for the chosen parameters.

Numerical models

The numerical models serve as a reference for the validation of the introduced analytical approach. For both geometric variants, horizontal pipe and planar trench collector, a separate model is set up in COMSOL Multiphysics (COMSOL Multiphysics® 2019). In both models, the Heat Transfer in Porous Media module is utilised, assigning a fluid phase and a solid matrix to characterise the porous structure. Furthermore, a local thermal equilibrium is applied and the effective conductivity of the porous medium is simulated as the weighted arithmetic mean (volume average) of the conductivities of the fluid and the solid matrix. Within the fully saturated porous medium, the liquid medium is designated as a phase change material, i.e., freezing is restricted to the fluid phase, while the solid matrix remains unaffected. The phase change within the fluid is modelled employing the apparent heat capacity method, applied over a transition interval of 2 K between phase 1 (ice) and phase 2 (water). Thus, the applied model accounts for the gradual freezing of the finite elements, it remains a simplification of all complex processes occurring in the soil while freezing. Nonetheless, it is adequately precise for this application. If complex thermo–hydro–mechanical processes are to be considered, e.g. soil uplift caused by frost, sophisticated models incorporating multiple physical processes such as described in Zhou and Meschke (2013) are to be applied. The collectors themselves are modelled as boundary heat sources and in their vicinity, where gradients are the biggest, the mesh is very fine and progressively gets coarser towards the boundaries. In a preliminary study, the influence on the accuracy of the element order on the temperature at collector wall and the maximum extension of the frozen soil was investigated. The temperature at the collector wall barely deviates (<0.02%) between a linear and a second-degree discretisation of the temperature. The maximum extension of the frozen soil on the other hand differs significantly within the first hours of ground freezing, but declines already within less than a day. Thereafter, the remaining deviation of the extension of the frozen soil is less than 1.3%. The significant discrepancy is due to a time shift in the onset of ground freezing and is irrelevant for the design of these systems. Given the minor differences between the linear and second-order discretisation and the fact that the simulation time increased by a factor of more than 18 for the second-order variant, further simulations were carried out using a linear temperature discretisation.

Horizontal pipe

The numerical model for the horizontal pipe is based on the parameters of the analytical model and is thus 2D as well. The horizontal pipe in the subsurface is represented by a circular void within a rectangular calculation region. Therefore, the heat extraction rate of the ILS model $\dot{q}_{\mathrm{ILS}}$ in W/m is to be converted into the heat flux density set in the numerical model in $\mathrm{W/m^2}$ to ensure equal conditions:

$$\dot{q}_{\mathrm{num}} = \frac{\dot{q}_{\mathrm{ILS}}}{2\pi r_{\mathrm{pipe}}} \tag{33}$$

The upper boundary of the rectangular calculation region represents the ground surface with the corresponding temperature boundary condition. The remaining boundaries of the domain are specified as adiabatic. The domain was defined empirically by varying its size, while both the accuracy of the temperature at the collector wall and at the border of the domain were monitored. At the left and right side, as well as at the lower border of the domain, so-called infinite regions are assigned to reduce the simulation domain while avoiding their boundary influencing the collector operation. The numerical calculation grid consists of a free triangle mesh extended by a structured mesh in the infinite regions. At the pipe boundary, the mesh resolution is significantly finer and gradually coarsens towards the outer regions. A figure of the mesh is provided in the "Appendix".

Planar trench collector

The numerical model of the planar trench collector is an extension of the numerical model described in Van de Ven et al. (2024). The collector is represented by a planar heat sink, i.e., the detailed geometry and internal flow dynamics of the collector are not considered. The computational domain was established through an empirical approach, involving systematic variation of its dimensions while monitoring both the collector wall temperature for different boundary conditions. To enhance computational efficiency, the numerical model applies two key simplifications: a quarter-domain approach using symmetry boundary conditions, and the implementation of infinite element domains at the outer boundaries. Together, these measures reduce the computational load while maintaining physical accuracy by eliminating boundary-induced effects at the collector wall. The mesh mainly consists of a free tetrahedral grid, which is supplemented by a structured mesh in the infinite element regions. A finer mesh is used near the collector surface to capture thermal gradients, while the element size increases gradually towards the domain boundaries. A figure of the mesh is provided in the "Appendix".

Results

Definition of scenarios for validation

The validation of the derived analytical model is carried out by comparison with the results of the numerical models. A period of 12 months is applied in all cases, as ground heat collectors need to be regenerated within this time frame to ensure consistent performance in the following period. The parameters employed for the

validation process for both the horizontal pipe and the planar trench collector are presented in Table 1. The subsequent analysis is conducted for three distinct scenarios: in scenario I, a constant temperature is imposed at the ground surface, with a constant heat extraction rate applied over the course of 1 year for both types of collectors. For scenario II, a seasonal temperature variation at the ground surface is introduced, while the heat extraction is reduced to 6 months to assess the natural regeneration process for both collector types. Finally, the most realistic conditions are represented in scenario III. This is implemented for the horizontal pipe model, where a load profile is applied alongside the actual temperature fluctuations at the ground surface. This load profile, representing typical conditions in the Northern Hemisphere, starts in October and ends in April (see Fig. 7).

The subsurface and collector properties used for the validation process are listed in Table 1. It is assumed that the soil is fully saturated. Although this is not always the case in practice, as the water content in the pore spaces increases after the phase transition, the assumption of complete saturation after the phase change is generally a close approximation of the actual conditions in humid climates such as in Central Europe.

Table 1 Collector and surface properties for the comparison of the analytical and numerical models

Subsurface properties			
Thermal conductivity of the solid matrix	λ_s	1.5	W/(m K)
Porosity	φ	0.25	
Density of the solid matrix	ρ_s	2180	kg/m^3
Specific heat capacity of the solid matrix	$c_{p,s}$	1000	J/(kg K)
Thermal conductivity of the groundwater	λ_w	0.58	W/(m K)
Density of the groundwater	ρ_w	1000	kg/m^3
Specific heat capacity of the groundwater	$c_{p,w}$	4200	J/(kg K)
Thermal conductivity of the ice	λ_{ice}	2.33	W/(m K)
Density of the ice	ρ_{ice}	900	kg/m^3
Specific heat capacity of the ice	$c_{p,ice}$	2000	J/(kg K)
Latent heat	h_{lat}	333,500	J/kg
Annual mean surface temperature	$T_{g,0}$	10	°C
Seasonal temperature oscillation			
Period	t_p	8760	h
Phase constant	t_0	840	h
Annual amplitude of the surface temperature	ΔT_{am}	10	K
Properties horizontal pipe			
Pipe radius	r_{pipe}	0.016	m
Installation depth	H_{inst}	1.2	m
Specific heat load rate	$\dot{q}_{tot}$	−20	W/m
Properties planar trench collector			
Collector length	L_c	7	m
Collector height	H_c	1.2	m
Collector thickness	d_c	0.006	m
Installation depth	H_{inst}	1.2	m
Specific heat load rate	$\dot{q}_{tot}$	−47.62	W/m^2

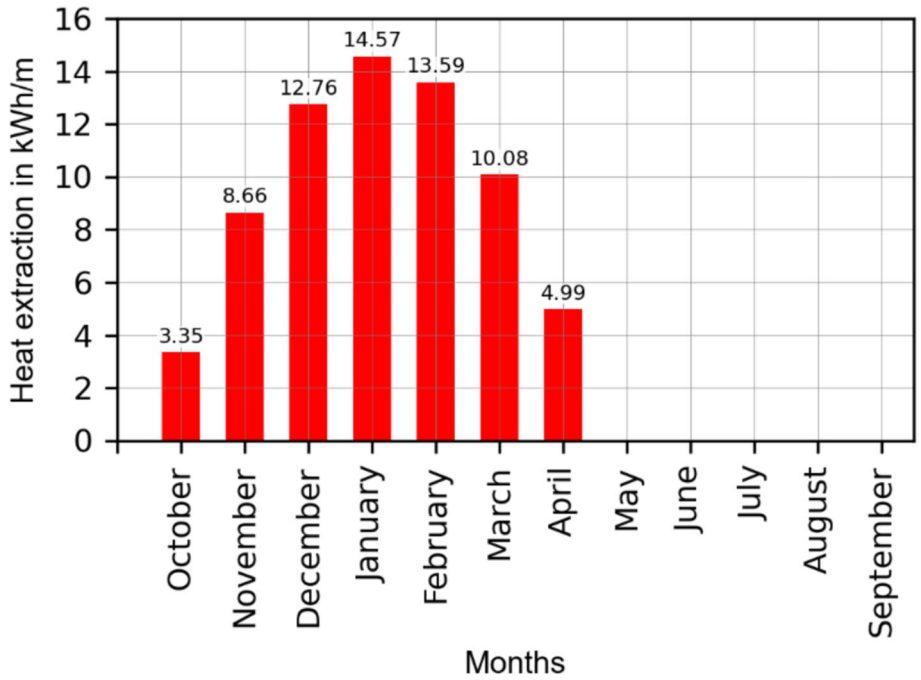

Fig. 7 Heat extraction profile used for the most realistic scenario III

To highlight the importance of considering soil freezing during the operation of ground heat collectors, additional numerical simulations without accounting for the phase change of the water content in the soil for all scenarios are presented while keeping all other conditions the same.

For the suitability of the analytical model as a design model, both design criteria, the collector outlet temperature and the maximum horizontal extent of the frozen ground, must be considered. Since the collector outlet temperature can rather precisely be determined based on the average collector wall temperature using resistance models for the mean fluid temperature and subsequently assuming a temperature spread over the collector length, results of the collector wall temperature of both models are compared with each other. Suitable analytical resistance models to determine the mean fluid temperature of the planar trench collector can be found in Van de Ven et al. (2024). In the case of a horizontal pipe, the analytical solution for heat conduction in concentric circles, presented in Eq. (25), can be applied to determine the mean fluid temperature. For the comparison of the maximum horizontal frozen extension, δ, between the analytical and numerical model, only the results for a collector wall temperature T_{cw} below -1 °C are considered. This is done, since in the analytical model, the phase change occurs at -1 °C, whereas in the numerical model, the phase change occurs between 0 and -2 °C.

Horizontal pipe

The first scenario (constant heat extraction rate and constant temperature at the surface) for the horizontal pipe model demonstrates excellent agreement for both examined parameters. It reveals a maximum deviation of 0.14 K for the collector wall temperature, T_{cw}, whereas the maximum horizontal extent of the frozen ground, δ, reaches a

maximum deviation of 1 mm or 10% (Fig. 8). If freezing of the soil was not considered, the mean temperature at the collector wall would be around 0.5 K lower. The comparison of computing times clearly demonstrates the advantage of the analytical model: with precalculated dimensionless temperatures as an input matrix, the analytical model takes less than 14 s of calculation time for this scenario, whereas the numerical models take 1 h and 2 min. Both calculations were executed for a time step size of 4 h on a machine equipped with an Intel® Core™ i7-6700 processor (8 logical cores at 3.40 GHz) and 38 GB RAM.

The results for the second scenario are shown in Fig. 9, where a constant heat extraction rate over 6 months is superposed with the temperature fluctuations at the ground surface. It has larger deviations in temperature at the collector wall, with a maximum absolute deviation of 0.60 K. The discrepancy in the maximum horizontal extent of the frozen ground is up to 5 mm, which corresponds to a deviation of 3% relative to the maximum frozen radius. This is notably smaller than the deviation in the previous scenario I. In this scenario, the freezing of the subsurface results in a maximum temperature change that is more than 2 K smaller than in the case without freezing.

The third scenario uses the extracted heat profile shown in Fig. 7 and also accounts for seasonal temperature fluctuations at the ground surface. It is assumed that the energy profile depicted in Fig. 7 is extracted continuously, i.e., a constant heat extraction rate is applied over each month. This scenario with a realistic heat extraction profile that is concentrated on the heating period reveals the largest deviations in both the temperature and the maximum extension, as depicted in Fig. 10. The largest temperature difference between the results of the numerical and analytical model is 1.33 K. The maximum

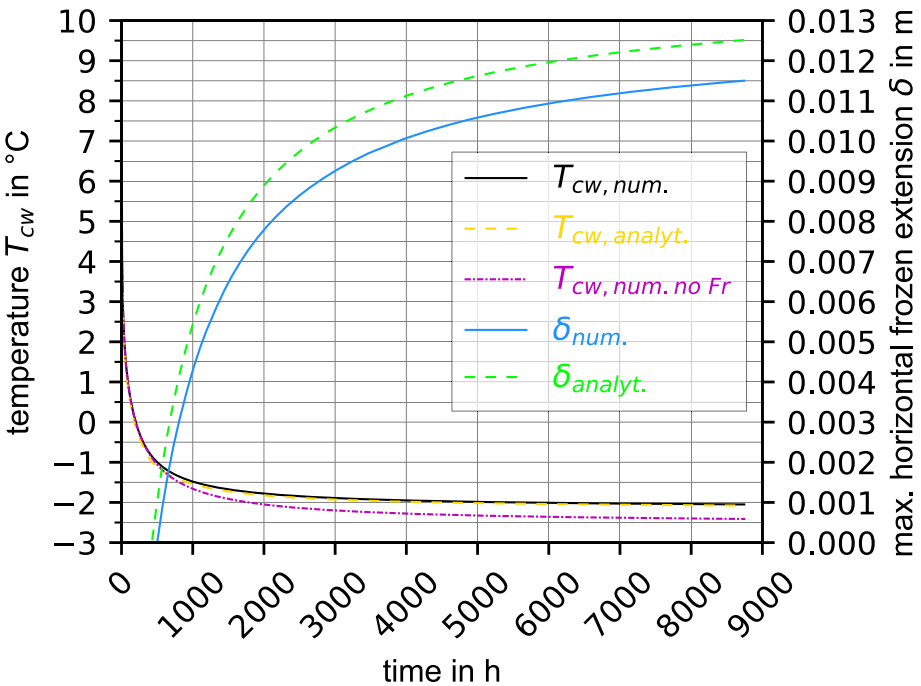

Fig. 8 Mean collector wall temperature and maximum horizontal extension of the frozen soil in scenario I, comparing the numerical and analytical simulations for a horizontal pipe

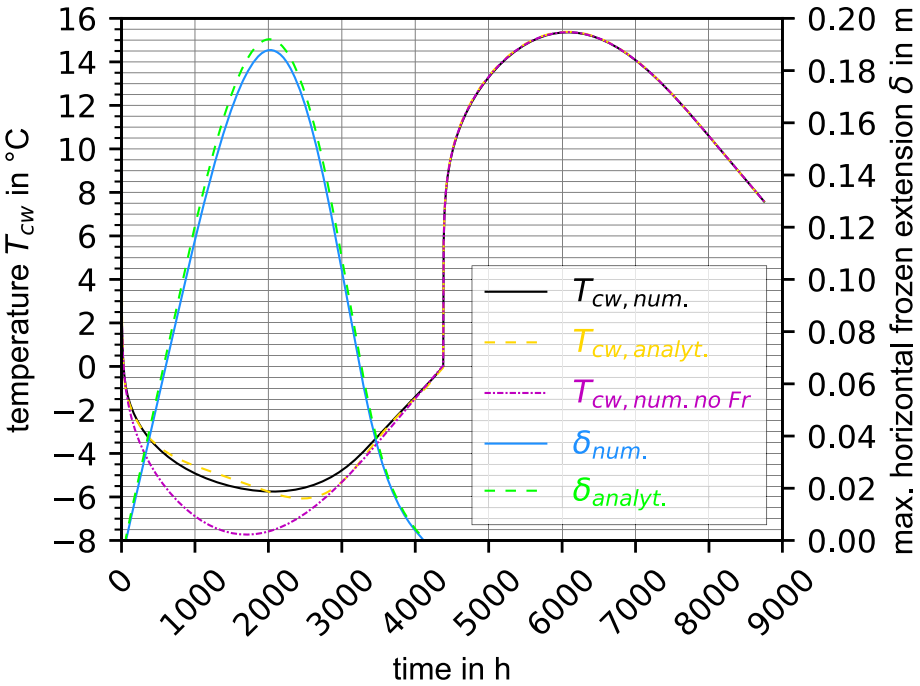

Fig. 9 Mean collector wall temperature and maximum horizontal extension of the frozen soil in scenario II, comparing the numerical and analytical simulations for a horizontal pipe

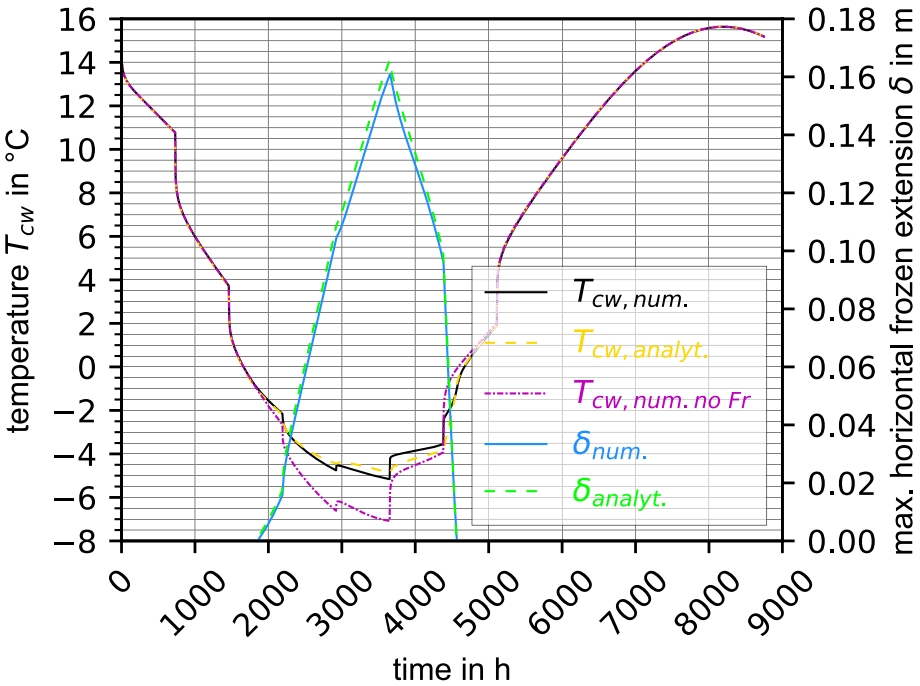

Fig. 10 Mean collector wall temperature and maximum horizontal extension of the frozen soil in scenario III, comparing the numerical and analytical model results for a horizontal pipe and assuming the heat extraction profile depicted in Fig. 7

frozen extension deviates up to 1.73 cm, which corresponds to 11% relative to the maximum extent of the frozen ground. A noticeable difference can also be observed in this scenario between the temperature at the collector wall if phase change in the soil is considered or not, again proving the influence of the freezing process.

Planar trench collector

Figure 11 shows the results for scenario I with a constant heat extraction rate and a constant temperature at the ground surface for the planar trench collector. The absolute temperature deviations are within a similar range as for the horizontal pipe model and reach a maximum of 0.80 K for the planar trench collector. The extent of the frozen ground deviates by up to 6.7 cm, which represents 13% relative to the maximum extent of the frozen ground with the most significant relative deviation occurring at the beginning of the transient state. However, towards the end of the simulation period of 1 year, the deviation decreases to 4%. Compared to the horizontal pipe results, accounting for the phase change in the surrounding soil has a larger impact on the temperature profile of the planar trench collector. The temperature difference between simulations with and without phase change in the soil is over 1 K larger for this collector type, making it roughly twice as large as for the horizontal pipe. The calculation time comparison for this collector is conducted in 48 h time steps. Similar to the horizontal pipe model, the analytical trench collector model also relies on precalculated dimensionless temperature responses and is executed on the same machine as the horizontal pipe calculations [Intel® Core™ i7-6700 processor (8 logical cores at 3.40 GHz); 38 GB RAM]. The computation takes around 0.14 s on

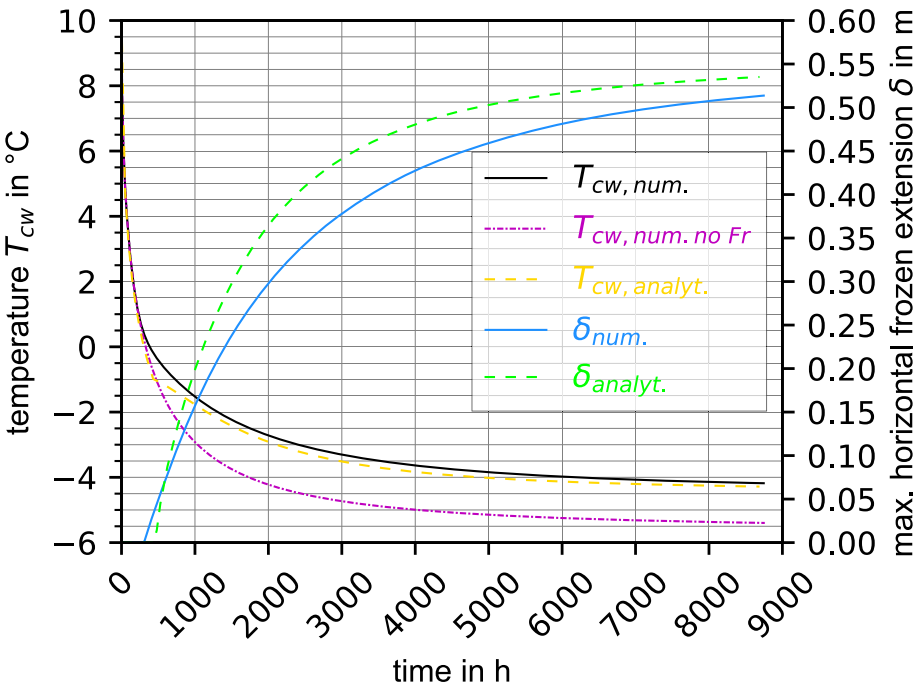

Fig. 11 Mean collector wall temperature and maximum horizontal extension of the frozen soil in scenario I, comparing the numerical and analytical model results for a planar trench collector

this machine, demonstrating the model´s efficiency. In contrast, the numerical model requires more than 13.5 h to run on a high-performance cluster with the cpu partition, one node and 32 tasks per node.

The results of both the analytical and numerical simulations for scenario II are shown in Fig. 12. At first sight, the analytical model seems to represent the numerical results less accurately as in the case of the horizontal pipe model. However, upon closer examination and consideration of the design parameters, there is a temporal shift of the maximum horizontal extension of the frozen ground and the temperature development during thawing. By comparison of the design-critical parameters, i.e., the overall minimum temperature and maximum horizontal extent of the frozen ground, the discrepancy is less significant. This specific consideration was neglected in the previous comparisons, as the overall agreement was regarded as satisfactory. The deviations of both parameters are visually emphasised in red in Fig. 12. The minimal temperature at the collector wall simulated with the analytical model is only 0.7 K lower than the numerical result. On the other hand, the maximum horizontal extension of the frozen ground is approximately 10 cm (or 14.4%) greater in the analytical solution. Both deviations lead to a more conservative estimation of the collector's performance, ensuring that no underdimensioning occurs. Without considering frost formation in the soil, the calculated temperature change would be more than 2 K greater than the one predicted by the proposed model, leading to a significant deviation from reality and an overly conservative design.

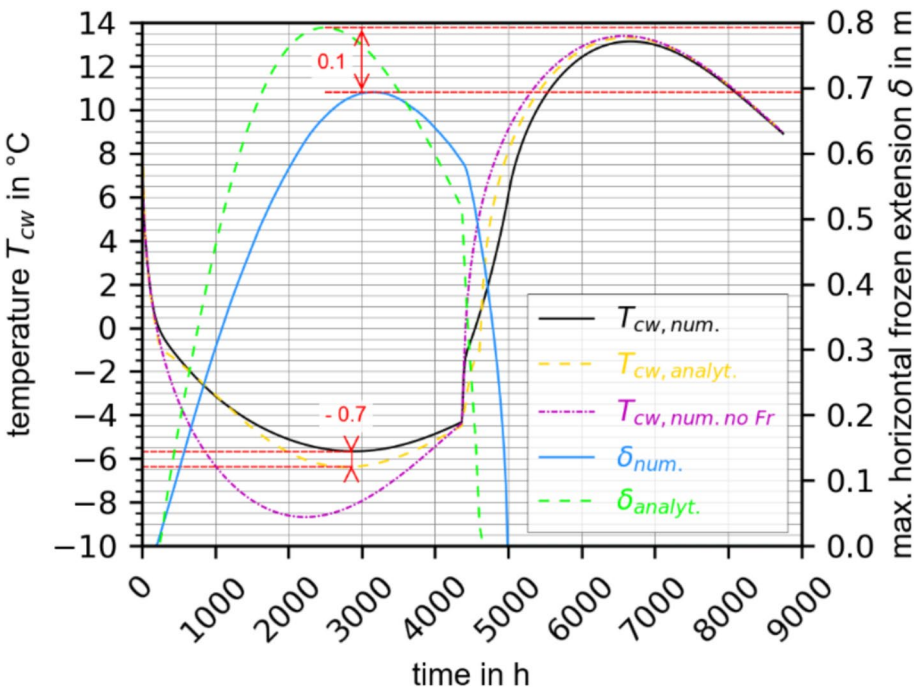

Fig. 12 Mean collector wall temperature and maximum horizontal extension of the frozen ground for scenario II, comparing both the numerical and analytical models for a planar trench collector

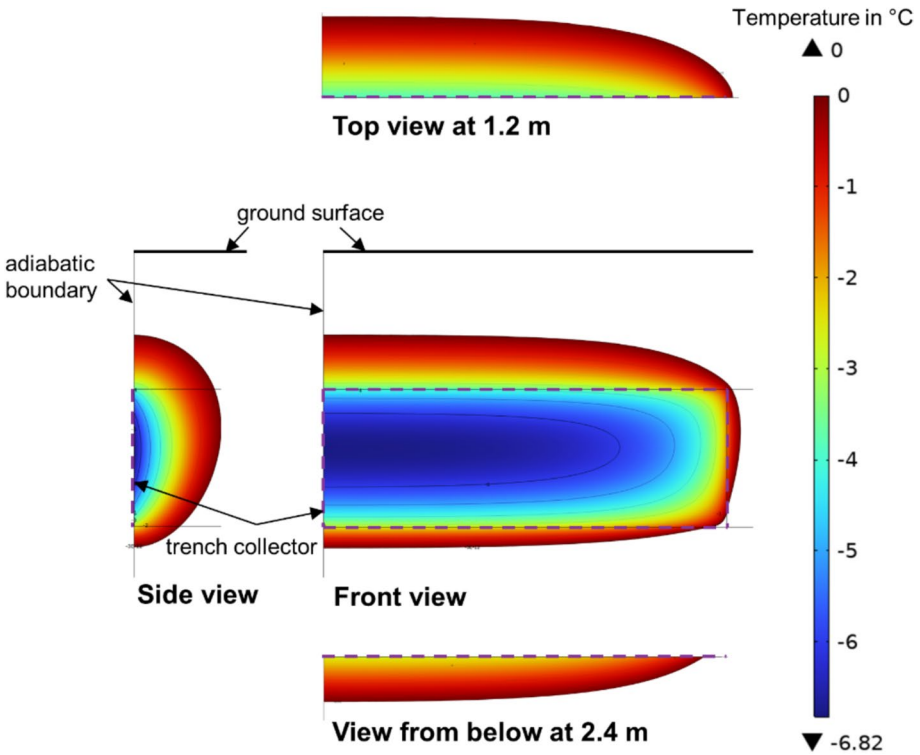

Fig. 13 Orthogonal projection of the temperature distribution around the planar trench collector of the second scenario after 2016 h of heat extraction

Discussion

The presented analytical modelling approach shows very good results for the mean collector wall temperature with deviations below 1.4 K for both analysed collector variants. Through the application of the dimensionless temperature response of the linear conduction problem, the dynamics of such temperature responses can be seamlessly preserved, even below the freezing temperature. This is achieved by adjusting the soil properties to account for the frozen state as soon as the freezing temperature is exceeded. Even though the temperature below the freezing point does not precisely match the numerical simulation, it is still sufficiently accurate, leaving little need for further adjustments.

However, the maximum extension of the frozen ground, especially for the planar trench collector, shows larger deviations of the analytical model compared to the numerical simulation. For the horizontal pipe, the deviation is not significant, ranging from a few millimetres to under 2 cm, and within a maximum range of approximately 10% for the investigated scenarios. Considering the temporal shift in the planar trench collector results, the deviation between the maximum horizontal extension of the frozen ground occurring in both models reaches a maximum of approximately 10 cm or 14%. To comprehend the greater discrepancy of the planar trench collector results, it is essential to analyse the frost expansion and the temperature distribution at the collector surfaces of the numerical simulations.

Figure 4 depicts the temperature distribution of the horizontal pipe investigated. It is clearly evident that the temperature distribution at the collector pipe wall is

homogeneous, and the temperature profile (and thus, the propagation of the frozen ground) expands outwards in a nearly radially symmetric manner. In addition, due to the model's 2D geometry, no secondary effects arise, such as temperature gradients at the pipe's inlet or outlet. Consequently, the shape factor of the analytical model corresponds very closely to the numerical results. The minor deviation in the maximum extent of the frozen ground can be attributed to the minimally asymmetric temperature and thus, frost distribution around the collector pipe.

Figure 13 shows the temperature distribution of the planar trench collector. It can be observed that the temperature distribution at the collector surface is pronounced non-uniform, with variations extending over a range greater than 6 K and even a small area with temperatures remaining above 0 °C. This significant temperature inhomogeneity, along with the non-uniform distribution of the frozen ground around the collector surface, complicates the determination of the correct frozen volume and its corresponding maximum extent.

Conclusions

This paper presents an analytical modelling methodology for geothermal heat collectors, which freeze the subsurface around them. The method is structured as follows:

- Up to the freezing temperature, solely an analytical source solution is used, which matches the corresponding collector geometry.
- Once the subsurface freezes, a thermal power balance is set up, consisting of the total extracted heat flow rate, the conductive heat flow rate from the surrounding ground, and the latent heat flow rate stored during the freezing process. The conductive heat flow rate is split up into so-called frozen and unfrozen components. The unfrozen component defines the conductive heat flow rate up to the frost temperature using unfrozen subsurface properties, whereas the frozen part is defined by the temperature difference between the frost temperature and the temperature at the collector wall of the previous time step and using frozen subsurface properties.
- The spatially averaged collector wall temperature is calculated by simple heat conduction equations over the distance between the source and the isotherm at freezing temperature. Since the extent of the frozen ground highly depends on the collector geometry, a suitable shape factor for each collector geometry has to be applied.
- The maximum extension of the frozen soil also highly depends on the collector geometry and consequently must be determined individually for each collector geometry under consideration.

The methodology outlined was applied to both a horizontal pipe configuration and a planar trench collector for various scenarios. All scenarios were subjected to a comparison with numerical results. The horizontal pipe model shows good agreement for both the collector wall temperature as well as the maximum extent of the frozen ground. With a deviation of around 10%, this model provides a solid foundation for the design of such systems. Considering the design-critical parameters, the planar trench collector model exhibits slightly higher deviations of up to 14% for the maximum extension of the frozen

ground. This is due to the more complex geometry and the non-homogeneous temperature distribution at the collector wall, and thus, directly influences the corresponding extent of the frozen ground. However, the collector wall temperature can be determined quite accurate with this model.

Thus, it can be concluded that the presented model approach is basically highly effective for the design of ground source heat collector systems, as the temperature at the collector wall can be determined with deviations of less than 1.4 K, while the accuracy for predicting the maximum extent of the frozen ground reaches at least 85.6%. For a horizontal pipe, the presented method enables accurate calculation of both the mean temperature at the collector wall and the extent of the frozen ground, making it suitable for the design of such systems. For the planar trench collector, the analytical model shows greater deviations but provides satisfactory results for the design of such systems. However, for a precise transient development of the collector wall temperature and the propagation of the frozen ground, the model used to determine the maximum horizontal extent of the frozen ground should be optimised. Furthermore, the current modelling approach does not yet account for adjacent collector pipes or collector plates within a ground-coupled heat pump system, which remains an area for future development.

Appendix

See Figs. 14 and 15.

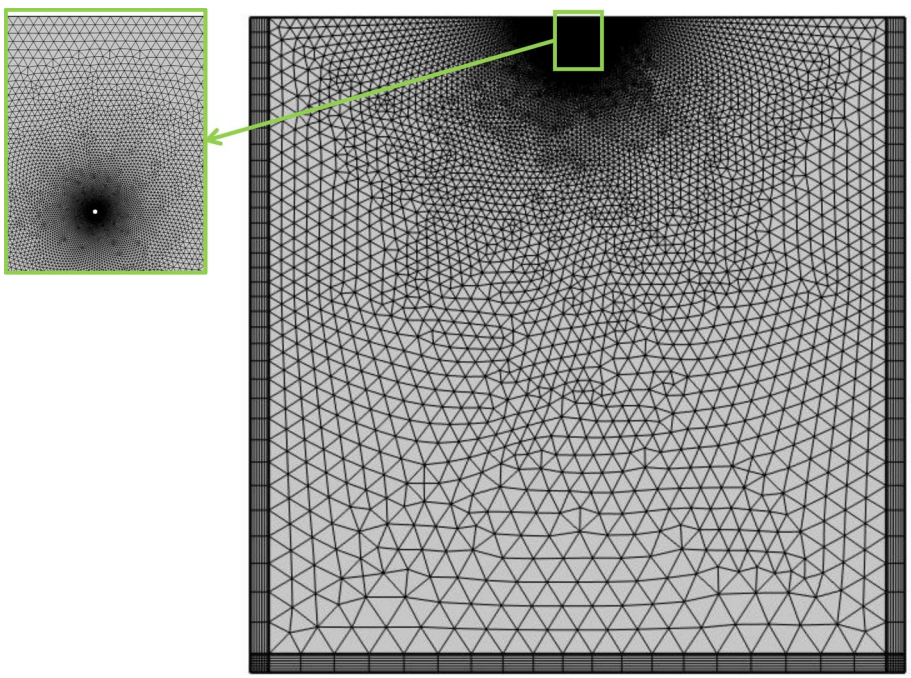

Fig. 14 Mesh of the numerical model of the horizontal pipe with a zoom of the vicinity of the heat source. The mesh consists of 29,880 elements and is extreme fine in the vicinity of the source

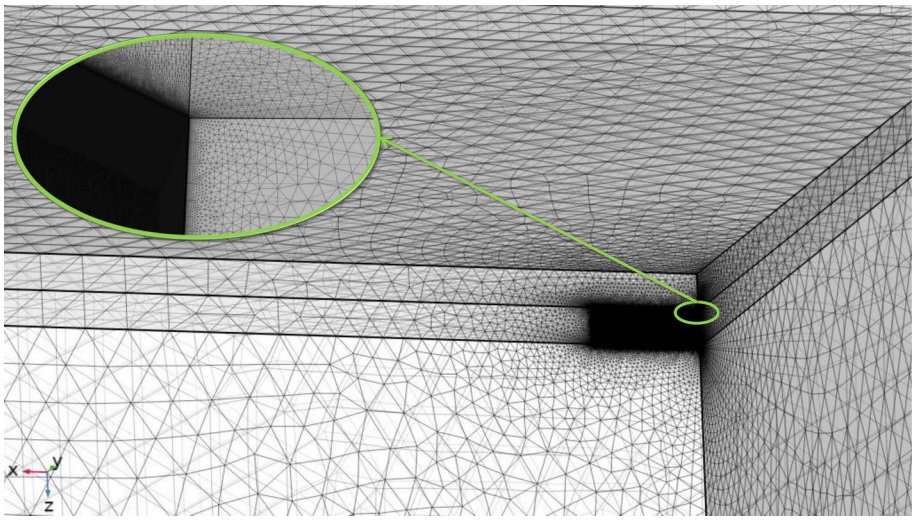

Fig. 15 Mesh of the numerical model of the planar trench collector with a zoom of the vicinity of the heat source. As the collector is only 6 mm thick, the mesh is extremely fine at the source. The mesh consists of 16,484,061 elements

Abbreviations

List of symbols

a (m^2/s)	Thermal diffusivity
A_{pipe} (m^2)	Cross-sectional area of the pipe
d (m K/W or m^2 K/W)	Dimensional factor of the dimensionless temperature response; phase-dependent soil properties are labelled accordingly by subscript
d_c (m)	Thickness of the trench collector
Fr (m^2 or m)	Amount of frozen soil representative of the model´s scale. In m^2 for the 2D model, and in m for the 3D model
h (J/kg)	Enthalpy
H (m)	Height or depth
L (m)	Length
n (–)	Number of the considered time step
$\dot{q}$(W/m or W/m^2)	Specific heat injection (positive) or extraction (negative) rate
r_{pipe} (m)	Radius of the collector pipe
S (–)	Shape factor of the frozen ground around the collector
t (s)	Time
t_0 (s)	Phase constant: time of the year at which the temperature of the ground surface reaches its minimum
T (°C)	Temperature
$\overline{T}_a$ (°C)	Annual mean air temperature
V (m^3)	Volume of the ground
x, y, z (m)	Space coordinates, where the temperature is evaluated

Abbreviations

2D	Two-dimensional
3D	Three-dimensional
BHE	Borehole heat exchanger
FPS	Finite plane source
ILS	Infinite line source

Greek symbols

δ (m)	Maximum, horizontal frozen distance between the collector wall and the frost isotherm
Δ	Change or interval of the physical quantity
θ (–)	Dimensionless temperature response
λ (W/m K)	Thermal conductivity
ρ (kg/m^3)	Density
φ (–)	Porosity of the subsurface

Subscripts

am	Referring to the annual amplitude at mean ground surface

analyst	Referring to the analytical results
c	Referring to the collector
cw	Referring to the collector wall
eq	Referring to the equivalent amount of the physical quantity
fr	Referring to the frozen properties
g,0	Referring to the undisturbed ground situation
hist	Referring to the history, i.e. to the previous time steps and its impact on the current time step
ice	Referring to the ice properties (frozen groundwater)
inst	Referring to the installation situation
lat	Referring to the latent heat of the physical quantity
no Fr	Referring to the simulations without phase change
num	Referring to the numerical results
p	Referring to the period
s	Referring to the properties of the solid matrix
tot	Referring to the total or overall amount of the physical quantity
unfr	Referring to the unfrozen properties
w	Referring to the groundwater properties
θ	Referring to the dimensionless response amount of the physical quantity

Superscript

′	Referring to the location of the source

Acknowledgements
We thank Michael Bachseitz for his work on the model development in the initial modelling phase and Stefan Hofmann for his support in calculus. We thank Ryan Pearson for proof reading.

Author contributions
Adinda Van de Ven: conceptualisation, methodology, software, validation, formal analysis, investigation, data curation, writing—original draft, visualisation, project administration, funding acquisition Peter Bayer: conceptualisation, writing—review & editing, supervision Roland Koenigsdorff: conceptualisation, methodology, writing—review & editing, supervision, project administration, funding acquisition.

Funding
Open Access funding enabled and organized by Projekt DEAL. Adinda Van de Ven is funded by the Federal Ministry of Economic Affairs and Climate Action of Germany within the framework of the research project Quality Enhancement of Shallow Geothermal Systems (QEWSplus) [grant number 03EE4020A]. Peter Bayer is supported by the EU Horizon Europe project INTERSTORES (project no. 101136100). Roland Koenigsdorff received no specific funding for this work.

Availability of data and materials
The data sets used during the current study are available from the corresponding author on reasonable request.

Declarations

Ethics approval and consent to participate
Not applicable.

Competing interests
The authors declare no competing interests.

Received: 18 April 2025 Accepted: 6 November 2025
Published online: 05 December 2025

References

Abdelaziz SL, Ozudogru TY, Olgun CG, Martin JR. Multilayer finite line source model for vertical heat exchangers. Geothermics. 2014;51:406–16. https://doi.org/10.1016/j.geothermics.2014.03.004.
Alzoubi MA, Zueter A, Nie-Rouquette A, Sasmito AP. Freezing on demand: a new concept for mine safety and energy savings in wet underground mines. Int J Min Sci Technol. 2019;29(4):621–7. https://doi.org/10.1016/j.ijmst.2019.06.015.
Arzanfudi MM, Al-Khoury R. Freezing-thawing of porous media: an extended finite element approach for soil freezing and thawing. Adv Water Resour. 2018;119:210–26. https://doi.org/10.1016/j.advwatres.2018.07.013.
Bahmani MH, Hakkaki-Fard A. A hybrid analytical-numerical model for predicting the performance of the horizontal ground heat exchangers. Geothermics. 2022;101:102369. https://doi.org/10.1016/j.geothermics.2022.102369.
Blocon AB. EED version 4—earth energy designer. 2020. https://www.buildingphysics.com/manuals/EED4.pdf. Accessed 1 Mar 2021.
Bottarelli M, Bortoloni M, Su Y, Yousif C, Aydın AA, Georgiev A. Numerical analysis of a novel ground heat exchanger coupled with phase change materials. Appl Therm Eng. 2015;88:369–75. https://doi.org/10.1016/j.applthermaleng.2014.10.016.
Carslaw HS, Jaeger JC. Conduction of heat in solids. 2nd ed. Oxford: Clarendon Press; 1959.

Cimmino M, Bernier M, Adams F. A contribution towards the determination of g-functions using the finite line source. Appl Therm Eng. 2013;51(1–2):401–12. https://doi.org/10.1016/j.applthermaleng.2012.07.044.
Ciriello V, Bottarelli M, Di Federico V, Tartakovsky DM. Temperature fields induced by geothermal devices. Energy. 2015;93:1896–903. https://doi.org/10.1016/j.energy.2015.10.052.
Claesson J, Dunand A. Heat extraction from the ground by horizontal pipes: a mathematical analysis. 1983.
COMSOL Multiphysics®. Stockholm, Schweden: COMSOL AB; 2019.
Erol S, François B. Multilayer analytical model for vertical ground heat exchanger with groundwater flow. Geothermics. 2018;71:294–305. https://doi.org/10.1016/j.geothermics.2017.09.008.
Eskilson P. Thermal analysis of heat extraction boreholes. PhD thesis, University of Lund, Sweden, Lund, Sweden. 1987.
Eslami-Nejad P, Bernier M. Freezing of geothermal borehole surroundings: a numerical and experimental assessment with applications. Appl Energy. 2012;98:333–45. https://doi.org/10.1016/j.apenergy.2012.03.047.
Fontaine P-O, Marcotte D, Pasquier P, Thibodeau D. Modeling of horizontal geoexchange systems for building heating and permafrost stabilization. Geothermics. 2011. https://doi.org/10.1016/j.geothermics.2011.07.002.
Gan G. Dynamic thermal modelling of horizontal ground-source heat pumps. Int J Low-Carbon Tech. 2013;8(2):95–105. https://doi.org/10.1093/ijlct/ctt012.
Giardina JJ. Evaluation of ground coupled heat pumps for the state of Wisconsin. Master thesis, University of Wisconsin-Madison, Wisconsin. 1995.
Glück B. Simulationsmodell "Erdwärmekollektor" zur wärmetechnischen Beurteilung von Wärmequellen, Wärmesenken und Wärme-Kältespeichern. 2009.
Gupta A, Loveridge F, Shafagh I, Rees S. An analytical approach to evaluate the heat transfer through the embedded retaining walls. In: EGEC. European geothermal congress; 18.10.2022–20.10.2022; Berlin. 2022.
Hirsch H, Petzold H, Grunewald J. Efficiency and area demand of multi-layer ground heat exchanger using phase change of water. In: EDP Sciences (Hg.). Fourth central European symposium on building physics. CESBP 2019, Prague, Czech Republic, 2–5.09.2019, 2027. 2019.
Huang S, Guo Y, Liu Y, Ke L, Liu G, Chen C. Study on the influence of water flow on temperature around freeze pipes and its distribution optimization during artificial ground freezing. Appl Therm Eng. 2018;135:435–45. https://doi.org/10.1016/j.applthermaleng.2018.02.090.
Huber A. Bedienungsanleitung zum Programm EWS. Huber Energietechnik AG, Zürich. 2016.
Hüsing F, Hirsch H, Rockendorf G. Combination of solar thermal collectors and horizontal ground heat exchangers as optimized source for heat pumps. In: International solar energy society; 11–14.10.2016; Palma de Mallorca, Spain. 2016. p. 1–11. https://doi.org/10.18086/eurosun.2016.04.18.
Hüsing F, Mercker O, Hirsch H, Kuntz DC, Walker-Hertkorn S, Sabel M. Erdwärmekollektoren und Sonnenkollektoren als optimierte bivalente Quelle für hocheffiziente Wärmepumpensysteme: Kurzbezeichnung: Terra-Solar-Quelle: gemeinsamer Abschlussbericht zum Verbundvorhaben: Laufzeit: 01.02.2015–31.03.2018. 2018. https://doi.org/10.2314/GBV:1047633868.
Incropera F, DeWitt DP, Bergman TL, Lavine AS. Principles of heat and mass transfer. 7th ed. Hoboken, NJ: Wiley; 2013.
Jeon J-S, Lee S-R, Kim M-J. A modified mathematical model for spiral coil-type horizontal ground heat exchangers. Energy. 2018;152:732–43. https://doi.org/10.1016/j.energy.2018.04.007.
Jiménez-Xamán C, Xamán J, Moraga NO, Hernández-Pérez I, Zavala-Guillén I, Arce J, et al. Solar chimneys with a phase change material for buildings: an overview using CFD and global energy balance. Energy Build. 2019;186:384–404. https://doi.org/10.1016/j.enbuild.2019.01.014.
Koenigsdorff R (2011) Oberflächennahe Geothermie für Gebäude: Grundlagen und Anwendungen zukunftsfähiger Heizung und Kühlung. Fraunhofer IRB-Verl., Stuttgart.
Kusuda T, Achenbach PR. Earth temperature and thermal diffusivity at selected stations in the United States. 1965.
Lamarche L. Horizontal ground heat exchangers modelling. Appl Therm Eng. 2019;155:534–45. https://doi.org/10.1016/j.applthermaleng.2019.04.006.
Lamarche L. Fundamentals of geothermal heat pump systems: design and application. 1st ed. Cham: Springer; 2023.
Li H, Nagano K, Lai Y. A new model and solutions for a spiral heat exchanger and its experimental validation. Int J Heat Mass Transfer. 2012a;55(15–16):4404–14. https://doi.org/10.1016/j.ijheatmasstransfer.2012.03.084.
Li H, Nagano K, Lai Y. Heat transfer of a horizontal spiral heat exchanger under groundwater advection. Int J Heat Mass Transfer. 2012b;55(23–24):6819–31. https://doi.org/10.1016/j.ijheatmasstransfer.2012.06.089.
Liu R, Zhang W, Han S, Du H, Cui P, Ma Z, et al. A numerical heat transfer model and performance evaluation of coaxial geothermal heat exchanger under soil freezing conditions. Appl Therm Eng. 2025;266:125538. https://doi.org/10.1016/j.applthermaleng.2025.125538.
Milagros Garcia Salciarini. Pump it down: why heat pump sales dropped in 2023. 2024. https://www.ehpa.org/wp-content/uploads/2024/04/Pump-it-down-why-heat-pump-sales-dropped-in-2023_EHPA_April-2024.pdf. Accessed 23 Jan 2025.
Molina-Giraldo N, Blum P, Zhu K, Bayer P, Fang Z. A moving finite line source model to simulate borehole heat exchangers with groundwater advection. Int J Therm Sci. 2011;50(12):2506–13. https://doi.org/10.1016/j.ijthermalsci.2011.06.012.
Ramming K. Bewertung und Optimierung oberflächennaher Erdwärmekollektoren für verschiedene Lastfälle. Dresden: TUD Press; 2007.
Spitler JD, Gehlin SE. Thermal response testing for ground source heat pump systems—an historical review. Renew Sustain Energy Rev. 2015;50:1125–37. https://doi.org/10.1016/j.rser.2015.05.061.
Spitler JD, Marshall CL, Manickam A, Dharapuram M, Delahoussaye RD, Yeung K-WD, et al. GLHEPro 5.0 for windows. 2016. https://hvac.okstate.edu/sites/default/files/pubs/glhepro/GLHEPRO_5.0_Manual.pdf. Accessed 1 Mar 2021.
Stauffer F, Bayer P, Blum P, Giraldo NM, Kinzelbach W. Thermal use of shallow groundwater. Boca Raton, FL: CRC Press; 2017.
Sutton MG, Nutter DW, Couvillion RJ. A ground resistance for vertical bore heat exchangers with groundwater flow. J Energy Resour Technol. 2003;125:183–9.

Urresta E, Moya M, Campana C, Cruz C. Ground thermal conductivity estimation using the thermal response test with a horizontal ground heat exchanger. Geothermics. 2021;96:102213. https://doi.org/10.1016/j.geothermics.2021.102213.
Van de Ven A, Koenigsdorff R, Hofmann S. Entwicklung konsistenter Auslegungsmodelle für oberflächennahe geothermische Quellensysteme. In: Karlsruher Institut für Technologie; 26–28.09.2018; Karlsruhe. 2018. p. 508–515.
Van de Ven A, Koenigsdorff R, Neth F, Zorn R, Schüppler S, Huttenloch P, et al. Advanced thermal and geophysical test methods of shallow geothermal systems. In: EGEC. European geothermal congress; 18.10.2022–20.10.2022; Berlin. 2022. p. 1–9.
Van de Ven A, Neth F, Kainzlsperger M, Koenigsdorff R. Thermal response tests an Erdwärmekollektoren. Geotherm Energ. 2023;104:12–5.
Van de Ven A, Bayer P, Koenigsdorff R. Analytical solution for the simulation of ground thermal conditions around planar trench collectors. Geothermics. 2024;124:1–14. https://doi.org/10.1016/j.geothermics.2024.103123.
VDI-Wärmeatlas: Mit 320 Tabellen. 11th ed. Berlin: Springer; 2013.
Verein Deutscher Ingenieure e.V. Thermische Nutzung des Untergrunds: Erdgekoppelte Wärmepumpenanlagen 06.2019. Berlin: Beuth Verlag GmbH: Beuth Verlag GmbH.
Wagner V, Blum P, Kübert M, Bayer P. Analytical approach to groundwater-influenced thermal response tests of grouted borehole heat exchangers. Geothermics. 2013;46(2):22–31. https://doi.org/10.1016/j.geothermics.2012.10.005.
Wang D, Lu L, Cui P. A new analytical solution for horizontal geothermal heat exchangers with vertical spiral coils. Int J Heat Mass Transf. 2016;100:111–20. https://doi.org/10.1016/j.ijheatmasstransfer.2016.04.001.
Westring P, Gibb D, Uguen G. European heat pump market and statistics report 2024. 2024. https://www.ehpa.org/market-data/. Accessed 23 Jan 2025.
Witte HJ, Heinrichs FA, Reichl C, Meeng C, Doerr C, Steuerer A, Kling S. Development and validation of analytical solutions for earth basket (spiral) heat exchangers. In: EGEC. European geothermal congress; 18.10.2022–20.10.2022; Berlin. 2022. p. 1–9.
Xiong Z, Fisher DE, Spitler JD. Development and validation of a Slinky™ ground heat exchanger model. Appl Energy. 2015;141:57–69. https://doi.org/10.1016/j.apenergy.2014.11.058.
Yang W, Kong L, Chen Y. Numerical evaluation on the effects of soil freezing on underground temperature variations of soil around ground heat exchangers. Appl Therm Eng. 2015;75:259–69. https://doi.org/10.1016/j.applthermaleng.2014.09.049.
Zhou MM, Meschke G. A three-phase thermo-hydro-mechanical finite element model for freezing soils. Int J Numer Anal Methods Geomech. 2013;37(18):3173–93. https://doi.org/10.1002/nag.2184.

Publisher's Note